WCSP'21 1570742121

CSI Ranging-based Wi-Fi Indoor Localization Error Analysis

Yuexin Long
School of Communication and Information Engineering
Chongqing University of Posts and Telecommunications
Chongqing, China
longyx98@foxmail.com

Mu Zhou
School of Communication and Information Engineering
Chongqing University of Posts and Telecommunications
Chongqing, China
zhoumu@cqupt.edu.cn

Zhenya Zhang
School of Communication and Information Engineering
Chongqing University of Posts and Telecommunications
Chongqing, China
zhenya_cqupt@foxmail.com

Wei Nie
School of Communication and Information Engineering
Chongqing University of Posts and Telecommunications
Chongqing, China
niewei@cqupt.edu.cn

***Abstract*—Compared with the Wi-Fi Received Signal Strength (RSS) commonly-used for the indoor localization, the Channel State Information (CSI) can be used for precise ranging to achieve the high Wi-Fi indoor localization accuracy since it includes the fine-grained physical-layer information such as the amplitude and phase of each subcarrier during the signal transmission. Due to the lack of the theoretical analysis of the localization error bound in the existing CSI ranging-based localization methods, it is not easy to compare the ideal performance of different localization methods. Therefore, this paper proposes a CSI ranging-based Wi-Fi indoor localization error bound analysis method, which is based on the indoor signal propagation model to derive out the CSI ranging-based localization error bound by considering the relationship between the localization accuracy and the path loss, shadow fading, multipath effect and asynchronous effect. Besides, through the experimental comparison, this paper analyzes the difference between the actual localization error and the derived localization error bound, as well as discusses the impact of different experimental parameters on the localization performance.**

***Index Terms*—Indoor localization, channel state information, Wi-Fi, localization error bound, ranging**

I. Introduction

At present, the Global Positioning System (GPS) and the cellular positioning system are two relatively mature outdoor positioning systems, which can provide the accurate and reliable location information for outdoor users. In contrast, the complexity of indoor structures, the movement of people, and the impact of obstructions cause indoor users to fail to receive signals from the GPS and cellular base stations effectively. The Wi-Fi indoor fingerprint localization system based on Received Signal Strength (RSS) has become the mainstream of indoor localization systems due to its wide signal coverage, low hardware requirement, and simple network deployment. However, due to the multipath effect in the indoor environment, the received RSS signal is unstable, the cost of building and maintaining the fingerprint database is relatively high, and the application of the system in the actual indoor environment is greatly restricted.

In response to the above problems, Wi-Fi indoor localization systems based on Channel State Information (CSI) ranging are beginning to gain the popularity. Compared with the RSS, the CSI contains finer-grained physical-layer information such as the amplitude and phase of each subcarrier, so it can be used for the Wi-Fi indoor localization and provide more accurate and stable localization results [1]. Due to the path loss, the shadow fading and multipath effect existing in the indoor environment cause the poor localization accuracy, Meanwhile, the clock asynchronous effect of hardware equipment is one of the main factors affecting the CSI-based localization accuracy, which is incurred by the crystal oscillating circuits in different devices and will incur a sampling frequency offset, so we need to analyze the impact of the above factors on the localization accuracy. To summarize, the two main contributions of this paper are listed as follows.

- The concept of the Cramer-Rao Lower Bound (CRLB) in the frequency domain is used to analyze the CSI ranging-based localization error, which solves the problem that the CRLB cannot be obtained without the Probability Density Function (PDF) of the CSI signal in the time domain.
- By considering the relationship between the localization accuracy and the path loss, shadow fading, multipath effect and asynchronous effect, the CSI ranging-based localization error bound is derived.

The rest of this paper is organized as follows. Some related works on the CSI indoor localization and localization error analysis are surveyed in Section II. The proposed system model is described in detail in Section III. Section IV derives out the closed-form expression of the proposed CRLB, and then Section V shows the related experimental results. Finally, Section VI concludes this paper and provides some future directions.

II. Related Work

Due to the rich physical layer information and high stability of the CSI, more and more scholars have conducted research on indoor localization methods based on CSI ranging. Authors in [2] use the channel splicing technology to continuously measure the CSI of multiple subcarriers in the channel coherence time, and then achieve the sub-meter-level ranging accuracy. Authors in [3] take the First Fresnel Zone (FFZ) as the prerequisite, establish the Power Fading Model (PFM) equation, and then estimate the target position by solving the PFM equation for all multipath signals. Authors in [4] use the Broadband Angle Ranging (BAR) method to estimate the propagation distance of the CSI signal, and then determine the target position by the trilateration method.

Specifically, the localization accuracy is affected by the path loss, shadow fading, and multipath effect in the indoor environment. Then, it is necessary to analyze the impact of the above factors on the localization performance. Authors in [5] derive out the Time of Arrival (TOA)-based localization error bound in the time domain, but it is obtained by an ideal signal propagation model and it is difficult to be applied to most actual indoor environments. Authors in [6] propose an indoor signal propagation model considering the multipath effect, by which the impact of the shadow fading and number of anchor nodes on the CSI localization error bound is analyzed. However, in this model, the multipath effect is simplified as an ideal Gaussian random variable, and thereby the diversity of the multipath signal is not considered, which makes the localization error bound deviate from the actual localization error significantly.

In this paper, considering the relationship between the indoor localization error bound and the environment factor such as the path loss, multipath effect, and noise power as well as the device factor such as the AP number, bandwidth and asynchronous effect, we derive out the closed-form expression of the CSI ranging-based indoor localization error bound, which can be used to investigate the ideal performance of the existing indoor localization methods.

III. System model

A. CSI signal model

Considered as the physical-layer information of the signal, the CSI contains the amplitude and phase information of each subcarrier that can be used to describe the attenuation and frequency deviation characteristics of the signal propagating from the transmitter to receiver. The signal amplitude attenuation occurs during the propagation process, and it is also affected by the multipath effect due to obstacles such as the floor, wall, and ceiling. Meanwhile, by considering the slow-speed pedestrian movement within the indoor environment, the Doppler frequency deviation of the signal ranging from 10 to 20 Hz can be ignored. Thus, the waveform of the received signal in the time domain can be represented as

$$r(t) = \sum_{i=1}^{l} a^{(i)} s(t - \tau^{(i)}) + z(t) \tag{1}$$

where $s(t)$ is the transmitted signal waveform, l is the number of propagation paths, $a^{(i)}$ and $\tau^{(i)}$ stand for the amplitude and propagation delay of the received signal respectively on the i-th propagation path, and $z(t)$ is the noise following the Gaussian distribution with the mean 0 and variance δ^2. After conducting the Analog-to-Digital Converter (ADC) transformation, the waveform of the received signal is converted into

$$r(nT) = \sum_{i=1}^{l} a^{(i)} s(nT - \tau^{(i)}) + z(nT) \tag{2}$$

with $n = 1, \cdots, L$, where T and L stand for the sampling period and number of sampling points respectively. Based on this, the waveform of the received signal at the m-th ($m = 1, \cdots, N$) Access Point (AP) can be represented as

$$r_m(nT) = \sum_{i=1}^{l} a_m^{(i)} s(nT - \tau_m^{(i)}) + z(nT) \tag{3}$$

with $n = 1, \cdots, L$, where $a_m^{(i)}$ and $\tau_m^{(i)}$ stand for the amplitude and propagation delay of the received signal respectively on the i-th propagation path at the m-th AP. Then, by conducting the L-point Discrete Fourier Transform (DFT) of $r_m(nT)$, the corresponding waveform of the received signal in the frequency domain can be obtained as

$$R_m(k) = \sum_{i=1}^{l} a_m^{(i)} S(k) e^{\frac{-j2\pi k \tau_m^{(i)}}{LT}} + \eta(k) \tag{4}$$

with $k = 0, \cdots, L-1$, where $S(k)$ and $\eta(k)$ stand for power spectrums of the transmitted signal and the noise following the Gaussian distribution with the mean 0 and covariance $L\delta^2$ respectively.

B. Error bound analysis model

According to the Fisher information theory [7], the CRLB is defined as the inverse of the Fisher Information Matrix (FIM), which describes the variance of the estimated value of unknown parameters. Different from the previous studies on the CSI ranging-based indoor localization error bound using the time-domain model [8], we rely on the frequency-domain model shown in (4), to derive out the error bound with the benefit of making the waveform information consistent with the practical capability of the Intel 5300 toolkit used for receiving the CSI. To achieve this goal, we set the expectation of the vector of $\boldsymbol{X} = (R_m(0), \cdots, R_m(L-1))^{\mathrm{T}}$ as $\boldsymbol{\mu} = \left(\overline{R_m(0)}, \cdots, \overline{R_m(L-1)}\right)^{\mathrm{T}}$ and the vector of parameters to be estimated as the 2-dimensional (2-D) coordinate of the pedestrian $\boldsymbol{\theta}=(\theta_1, \theta_2)^{\mathrm{T}}$, where $\overline{R_m(k)}$ is the expectation of $R_m(k)$ and T is the transpose operation. and then the element on the i-th row and j-th column in the FIM with respect to $\boldsymbol{\theta}$ is then calculated as

$$I_{ij} = 2\mathrm{Re}\left[\frac{\partial \boldsymbol{\mu}^{\mathrm{H}}}{\partial \theta_i} \boldsymbol{\Sigma}^{-1} \frac{\partial \boldsymbol{\mu}}{\partial \theta_j}\right], i, j = 1, 2 \tag{5}$$

where Re and H are real-part and matrix conjugate transpose operations, $\boldsymbol{\Sigma} = L\delta^2 \boldsymbol{E}$ is the covariance matrix of $\boldsymbol{X}$, and $\boldsymbol{E}$

is the identity matrix. Based on this, the error bound equals to $V_{\boldsymbol{\theta}} = (I_{11}+I_{12})/\left(I_{11}I_{22} - I_{12}^2\right)$.

IV. CRLB ANALYSIS

A. Error Estimation with Clock Synchronization

According to (4), the parameters to be estimated in the frequency domain expression of the received signal waveform can be represented as $\boldsymbol{\theta} = \left(a_1^{(1)}, \tau_1^{(1)}, \cdots, a_1^{(l)}, \tau_1^{(l)}, \cdots, a_N^{(1)}, \tau_N^{(1)}, \cdots, a_N^{(l)}, \tau_N^{(l)}\right)^{\mathrm{T}}$. To derive out the CSI ranging-based indoor localization error bound, we propose the association of parameters. Firstly, we set 2-D coordinates of the target and the m-th AP as (x, y) and (x_m, y_m) respectively, and calculate the distance between them as $d_m = \sqrt{(x_m - x)^2 + (y_m - y)^2}$.

According to the random weighting theory [6], we have

$$\tau_m^{(i)} = \frac{\lambda_m^{(i)}\sqrt{(x_m - x)^2 + (y_m - y)^2}}{v} \tag{6}$$

where v is the speed of light and $\lambda_m^{(i)} (\in [1, 20))$ is the weighting factor of the i-th propagation path at the m-th AP, and meanwhile

$$a_m^{(i)} = \frac{a_0}{\lambda_m^{(i)}\sqrt{(x_m - x)^2 + (y_m - y)^2}}\varepsilon^{p_m^{(i)}} \tag{7}$$

where a_0 is the amplitude of the received signal at the location with 1 m from the transmitter (or called the reference location), $\varepsilon (\in (0, 1))$ is the environment coefficient, and $p_m^{(i)}$ is the number of reflections of the signal on the i-th propagation path at the m-th AP.

According to (6) and (7), we can find that the estimation of $\boldsymbol{\theta}$ is equivalent to the estimation of $\boldsymbol{\theta'} = (x, y)$, then the waveform of the received signal at the m-th AP can be represented as

$$r_m(t) = \sum_{i=1}^{l} \frac{a_0\varepsilon^{p_m^{(i)}}}{\lambda_m^{(i)} d_m} s(t - \frac{\lambda_m^{(i)} d_m}{v}) + z(t) \tag{8}$$

By conducting the L-point DFT of $r_m(t)$, the corresponding frequency domain can be obtained as

$$R_m(k) = \sum_{i=1}^{l} \frac{a_0\varepsilon^{p_m^{(i)}} S(k) e^{\frac{-j2\pi k\lambda_m^{(i)} d_m}{LTv}}}{\lambda_m^{(i)} d_m} + \eta(k) \tag{9}$$

From (5), by setting the expectation of the vector of observations $\boldsymbol{X} = \left(R_m^{(i)}(0), \cdots, R_m^{(i)}(k), \cdots, R_m^{(i)}(L-1)\right)^{\mathrm{T}}$ as $\boldsymbol{\mu} = \left(\overline{R_m^{(i)}(0)}, \cdots, \overline{R_m^{(i)}(k)}, \cdots, \overline{R_m^{(i)}(L-1)}\right)^{\mathrm{T}}$, where $\overline{R_m^{(i)}(k)}$ is the expectation of $R_m^{(i)}(k)$, the FIM with respect to $\boldsymbol{\theta'}$ is constructed as

$$\mathbf{I}_{\boldsymbol{\theta'}} = \frac{2a_0^2}{L\delta^2} \sum_{m=1}^{M} H_m \mathbf{D}_m \tag{10}$$

where

$$H_m = \sum_{i=1}^{l}\sum_{k=0}^{L-1} |S(k)|^2 \left(\frac{1}{d_m^4 \left(\frac{\lambda_m^{(i)}}{\varepsilon^{p_m^{(i)}}}\right)^2} + \frac{4\pi^2 k^2}{L^2 v^2 T^2 d_m^2 \left(\frac{1}{\varepsilon^{p_m^{(i)}}}\right)^2}\right) \tag{11}$$

$$\boldsymbol{D}_m = \begin{bmatrix} \cos\theta_m^2 & cos\theta_m \sin\theta_m \\ \sin\theta_m cos\theta_m & \sin\theta_m^2 \end{bmatrix} \tag{12}$$

and $|S(k)|$ is the amplitude of the transmitted signal.

Finally, the CSI ranging-based indoor localization error bound is derived as (13).

B. Error Estimation with Clock Asynchronization

The phase deviation of the frequency signal introduced by the difference of hardware devices causes a fixed time offset τ_0 between the actual sampling time of the AP and the optimal sampling time, that is, the clock asynchronous effect. According to (6)-(8), we can represent the waveform of the received signal with the asynchronous effect at the m-th AP as

$$\tilde{r}_m(nT) = \sum_{i=1}^{l} a_m^{(i)} s(nT - \tau_m^{(i)} - \tau_0) + z(t), \tag{14}$$

where $n = 1, \cdots, L$. Then, by conducting the L-point Discrete Fourier Transform (DFT) of $\tilde{r}_m(nT)$, the corresponding waveform of the received signal in the frequency domain can be obtained as

$$\tilde{R}_m(k) = \sum_{i=1}^{l} a_m^{(i)} S(k) e^{\frac{-j2\pi k\left(\tau_m^{(i)} + \tau_0\right)}{LT}} + \eta(k), \tag{15}$$

where $k = 0, \cdots, L-1$. In this case, the vector of parameters to be estimated can be obtained as $\tilde{\boldsymbol{\theta}} = \left(a_1^{(1)}, \tau_1^{(1)}, \cdots, a_1^{(l)}, \tau_1^{(l)}, \cdots, a_N^{(1)}, \tau_N^{(1)}, \cdots, a_N^{(l)}, \tau_N^{(l)}, \tau_0\right)^{\mathrm{T}}$. There are not only parameters x and y to be estimated for target positioning, but also the time offset τ_0 caused by the clock asynchronous effect.

Then, according to (5), the FIM with respect to $\tilde{\boldsymbol{\theta}}$ is constructed as

$$\mathbf{I}_{\tilde{\theta}} = \begin{bmatrix} \mathbf{A} & \mathbf{B} \\ \mathbf{B^T} & \mathbf{C} \end{bmatrix}, \tag{16}$$

where

$$\mathbf{A} = \begin{bmatrix} \sum\limits_{m=1}^{M} H_m \cos\theta_m^2 & \sum\limits_{m=1}^{M} H_m \cos\theta_m \sin\theta_m \\ \sum\limits_{m=1}^{M} H_m \sin\theta_m \cos\theta_m & \sum\limits_{m=1}^{M} H_m \sin\theta_m^2 \end{bmatrix}, \tag{17}$$

$$\mathbf{B} = \begin{bmatrix} \sum\limits_{m=1}^{M} \frac{Y_m \cos\theta_m}{v} & \sum\limits_{m=1}^{M} \frac{Y_m \sin\theta_m}{v} \end{bmatrix}^{\mathrm{T}}, \tag{18}$$

$$\mathbf{C} = \sum_{m=1}^{M} Y_m, \tag{19}$$

where $Y_m = \sum\limits_{i=1}^{l}\sum\limits_{k=1}^{L-1} |S(k)|^2 \frac{4\pi^2 \left(\varepsilon^{p_m^{(i)}}\right)^2 k^2}{\left(\lambda_m^{(i)}\right)^2 d_m^2 L^2 T^2}$.

Since we are interested in the location information of the target, which can be obtained from the equivalent Fisher

$$V_{\boldsymbol{\theta}'} = \mathrm{tr}\left\{\mathbf{I}_{\boldsymbol{\theta}'}^{-1}\right\} = \frac{L\delta^2}{2a_0^2} \frac{\sum_{m=1}^{M} H_m}{\left(\sum_{m=1}^{M} H_m \cos^2\theta_m\right)\left(\sum_{m=1}^{M} H_m \sin^2\theta_m\right) - \left(\sum_{m=1}^{M} H_m \cos\theta_m \sin\theta_m\right)^2} \tag{13}$$

information matrix (EFIM), we rely on [9] to construct the EFIM with respect to $\tilde{\boldsymbol{\theta}}$ as

$$\mathbf{I}_E = \mathbf{A} - \mathbf{B}\mathbf{C}^{-1}\mathbf{B}^{\mathbf{T}}, \tag{20}$$

which has the property that $\left[\mathbf{I}_{\tilde{\boldsymbol{\theta}}}^{-1}\right]_{2\times 2} = \mathbf{I}_E^{-1}$, where $[\cdot]_{n\times n}$ represents the submatrix of the first n rows and first n columns of matrix, and then the CSI-based indoor localization error bound with the asynchronous effect considering the pedestrian motion is derived as

$$V_{\tilde{\boldsymbol{\theta}}} = \mathrm{tr}\left\{\mathbf{I}_E^{-1}\right\} = \frac{L\delta^2}{2a_0^2} \frac{I_4}{I_1 I_2 - {I_3}^2}, \tag{21}$$

where $I_1 = \sum_{m=1}^{N} H_m \cos^2(\theta_m) - \frac{\left(\sum_{m=1}^{N} Y_m \cos\theta_m\right)^2}{v^2 \sum_{m=1}^{N} Y_m}$, $I_2 = \sum_{m=1}^{N} H_m \sin^2(\theta_m) - \frac{\left(\sum_{m=1}^{N} Y_m \sin\theta_m\right)\left(\sum_{m=1}^{N} Y_m \sin\theta_m\right)}{v^2 \sum_{m=1}^{N} Y_m}$, $I_3 = \sum_{m=1}^{N} H_m \sin\theta_m \cos\theta_m - \frac{\left(\sum_{m=1}^{N} Y_m \cos\theta_m\right)\left(\sum_{m=1}^{N} Y_m \sin\theta_m\right)}{v^2 \sum_{m=1}^{N} Y_m}$, $I_4 = \sum_{m=1}^{N} H_m - \frac{\left(\sum_{m=1}^{N} Y_m \cos\theta_m\right)^2 + \left(\sum_{m=1}^{N} Y_m \sin\theta_m\right)^2}{v^2 \sum_{m=1}^{N} Y_m}$.

V. Experimental Results

As shown in Fig. 1, in a real indoor environment with dimensions of 49.3 m by 17.8 m, we calculate the CSI ranging-based localization error bound, and then compare it with the actual localization error by the method in [10] to verify the effectiveness of the proposed method. There are in total 8 APs (i.e., the Intel 5300 toolkit, notated from AP1 to AP8) randomly deployed in this environment to receive the signal from the transmitter (i.e., the TP-LINK TL-WR2041N) at the target location. For simplicity, we assume that the noise power is from -95 dBm to -75 dBm, the received signal power at the reference location is -40 dBm, and the bandwidth varies from 60 MHz to 300 MHz.

Fig. 2 shows the actual localization error and proposed localization error bound with different noise power. This result shows that with the variation of the noise power, both of them have the similar variation trend, which verifies the effectiveness of the proposed localization error bound in describing the CSI ranging-based Wi-Fi indoor localization performance. However, due to the complexity and unpredictability of the actual environmental noise, there is a certain difference in the absolute value of the actual localization error and proposed localization error bound.

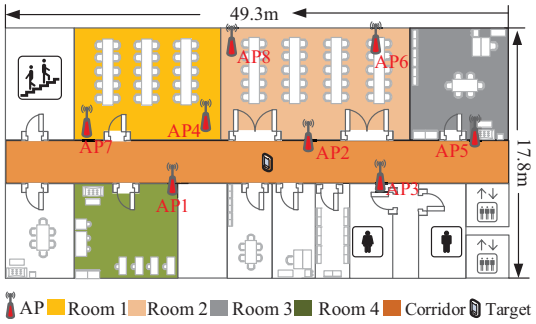

Fig. 1. Environmental layout.

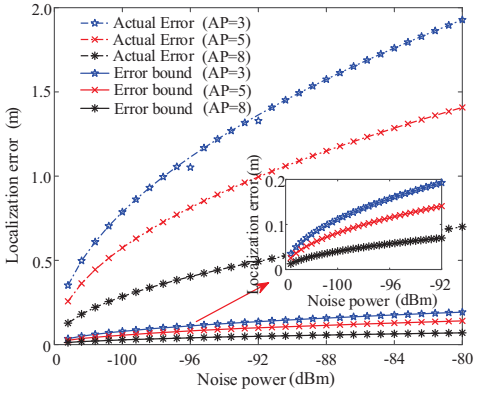

Fig. 2. Error bound vs. actual error with different noise power.

Fig. 3 gives the actual localization error and proposed localization error bound with different bandwidth. It can be observed that with the increase of the bandwidth, both the actual localization error and proposed localization error bound are in a downward trend, especially in the case of the small bandwidth, the variation trend is obvious since the increase of the bandwidth improves the time resolution, and consequently enhances the direct path resolution capability at the AP. In addition, the effect of the increased bandwidth on the localization performance shows a convergence trend, and in the case of the large bandwidth, the variation of the bandwidth does not have significant effect on the localization performance.

As shown in Fig. 4, which compares the actual localization error with proposed localization error bound in different indoor environments. This result indicates that the proposed localization error bound has the similar variation trend to the actual localization error, and meanwhile it can effectively characterize the relative relationship of the localization error in different indoor environments.

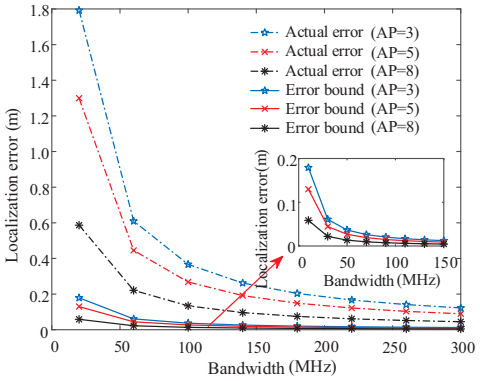

Fig. 3. Error bound vs. actual error with different bandwidth.

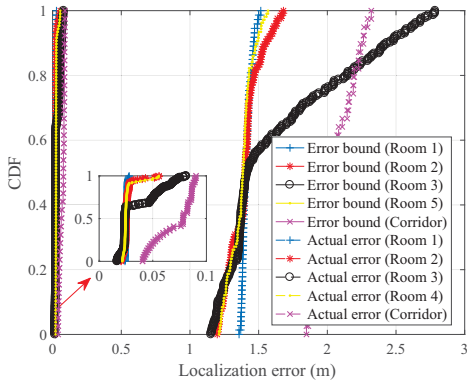

Fig. 4. Error bound vs. actual error with different indoor structures.

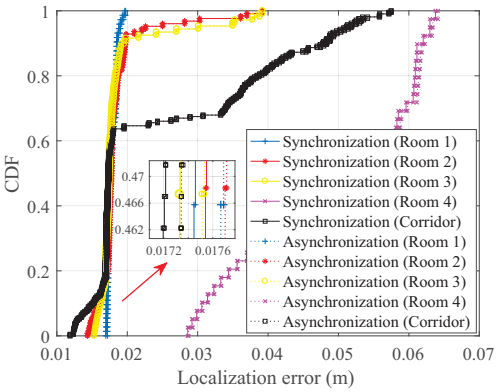

(a) Error bound

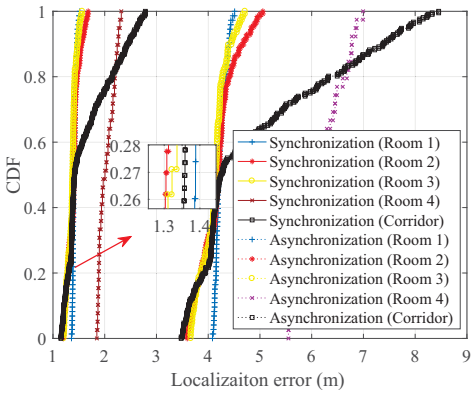

(b) Actual error

Fig. 5. Error bound vs. actual error with clock synchronization and ansychronization.

Finally, Fig. 5(a) and Fig. 5(b) show the localization error bound and actual localization error with the clock synchronization and asynchronization respectively. It can be observed that the clock asynchronous effect has a negative impact on the localization accuracy especially for the actual environment. Therefore, the clock asynchronous effect should be eliminated as much as possible for the sake of achieving the high-precision localization.

VI. Conclusion

This paper derives out the CSI ranging-based Wi-Fi indoor localization error bound and analyzes the impact of different factors on the localization error bound. Experimental results show that given the noise power, the increase of the AP number and bandwidth can reduce the localization error. Meanwhile, the change of the indoor environment and clock asynchronization also affect the localization performance. In the future, we will focus on multipath signal modeling and analyzing the impact of the device difference on the localization error bound.

Acknowledgment

This work is supported in part by the National Natural Science Foundation of China (61771083, 61704015), Program for Changjiang Scholars and Innovative Research Team in University (IRT1299), and Postgraduate Scientific Research and Innovation Project of Chongqing (CYS21293).

References

[1] R. Ma, G. Yu, G. Chen, and et al, "Hierarchical CSI-fingerprints classification for passive multi-person localization," *International Conference on Networking and Network Applications (NaNA)*, pp. 112-117, 2017.

[2] Y. Xie, Z. Li, and M. Li, "Precise power delay profiling with commodity Wi-Fi," *IEEE Transactions on Mobile Computing*, vol. 18, no. 6, pp. 1324-1355, 2018.

[3] J. Wang, J. Xiong, H. Jiang, and et al, "Low human-effort, device-free localization with fine-grained subcarrier information," *IEEE Transactions on Mobile Computing*, vol. 17, no. 11, pp. 2550-2563, 2018.

[4] S. Han, Y. Li, W. Meng, and et al, "Indoor localization with a single Wi-Fi access point based on OFDM-MIMO," *IEEE Systems Journal*, vol. 13, no. 1, pp. 964-972, 2018.

[5] N. Patwari, A. O. Hero, M. Perkins, and et al, "Relative location estimation in wireless sensor networks," *IEEE Transactions on Signal Processing*, vol. 51, no. 8, pp. 2137-2148, 2003.

[6] L. Gui, M. Yang, H. Yu, and et al, "A Cramer-Rao Lower Bound of CSI-based indoor localization," *IEEE Transactions on Vehicular Technology*, vol. 67, no. 3, pp. 2814-2818, 2018.

[7] S. K. Sengijpta, "Fundamentals of statistical signal processing: Estimation theory," *Technometrics*, vol. 37, no. 4, pp. 465-466, 1995.

[8] M. Zhou, F. Qiu, K. Xu and et al, "Error bound analysis of indoor Wi-Fi location fingerprint based positioning for intelligent access point optimization via Fisher information," *Computer Communications*, vol. 86, no. 15, pp. 57-74, 2016.

[9] Y. Shen and M. Z. Win, "Fundamental Limits of Wideband Localization-Part I: A General Framework," *IEEE Transactions on Information Theory*, vol. 56, no. 10, pp. 4956-4980, 2010.

[10] M. Kotaru, K. Joshi, D. Bharadia, and et al, "SpotFi: Decimeter level localization using WiFi," *Computer Communication Review*, vol. 45, no. 4, pp. 269-282, 2015.